THE WEAKLY NONLINEAR MAGNETOROTATIONAL INSTABILITY IN A THIN-GAP TAYLOR COUETTE FLOW

CLARK, S.E.[1] AND OISHI, J.S. [2,3]
Draft version October 3, 2016

ABSTRACT

The magnetorotational instability (MRI) is a fundamental process of accretion disk physics, but its saturation mechanism remains poorly understood. We present an analytic analysis of the nonideal MRI in the weakly nonlinear regime – that is, when the MRI system is just unstable to its most unstable mode.

1. INTRODUCTION

For matter to accrete from a disk onto a central object, angular momentum must be transported radially outward in the disk. The transport mechanism is likely turbulent, as molecular viscosity alone cannot account for the needed angular momentum transfer, and likely magnetic, as this turbulence is excited even in hydrodynamically stable disks (Shakura & Sunyaev 1973). Since its discovery by Chandrasekhar (1960) and subsequent rediscovery by Balbus & Hawley (1991), the magnetorotational instability (MRI) remains the leading explanation for rapid angular momentum transport in astrophysical disks. The instability in its simplest geometry arises when a differentially rotating disk is threaded by a vertical magnetic field. The presence of the magnetic field linearly destabilizes the disk gas, driving turbulence and angular momentum transport. The MRI likely plays a role in a diverse host of astrophysical systems, including protoplanetary disks and black hole accretion disks, as well as stellar interiors. Despite its importance, many aspects of the MRI remain poorly understood. In particular, the nonlinear saturation mechanism for the MRI is an open question, and a formidable challenge. MRI saturation has been tackled almost exclusively with simulation, with a few notable exceptions detailed below. In this work we investigate the weakly nonlinear behavior of the MRI.

Weakly nonlinear analysis is a perturbative method used to examine the asymptotic behavior of a system near threshold – that is, when the system is just barely unstable to its most unstable mode. The analytical technique follows the multiscale evolution of fluid variables in a perturbation expansion, allowing the controlled interaction of modes between orders in a perturbation series (see, e.g., Bender & Orszag for a full mathematical formalism). Weakly nonlinear analysis can be a powerful technique for analytically examining systems which in their full generality exhibit such complicated nonlinear behavior that their study is relegated primarily to the simulation domain. The MRI is one such phenomenon: while there is a rich literature analytically examining the linear MRI, analytical treatments of the *nonlinear* system are relatively few. The weakly nonlinear treatment of the MRI was pioneered by Umurhan et al. (2007a, 2007b; hereafter URM07). The authors undertook the first weakly nonlinear analysis of the MRI in a thin-gap Taylor Couette flow, and found that the marginal MRI system approaches saturation in a manner analogous to that of Rayleigh-Bénard convection. Weakly nonlinear analysis was instrumental in our understanding of Rayleigh-Bénard convection saturation (Newell & Whitehead 1969), and the similarities between convection and the thin-gap MRI are the result of important shared symmetries between the systems. The success of URM07 in modeling the MRI system near threshold merits further consideration, but we are unaware of any other attempts to expand upon their theoretical framework. In this work we rigorously rederive the theory of URM07, and expand upon their findings. Our focus here is on fully characterizing the narrow gap MRI system, both for independent theoretical interest and to have a robust comparison point for extensions of this theory into more complicated geometries. In a companion paper we derive for the first time the weakly nonlinear theory of the standard and helical MRI in a wide gap Taylor Couette flow (Clark & Oishi 2016b, hereafter Paper II). The thin- and wide-gap treatments complement one another theoretically, and both are important regimes for comparison with simulation.

This work examines Taylor Couette flow in the thin-gap regime, an idealization in which the radial extent of the channel is very small compared to its distance from the center of rotation, i.e. $(r_2 - r_1) \ll \frac{1}{2}(r_1 + r_2)$ where r_1 and r_2 are the radii of the inner and outer flow boundaries, respectively. The thin-gap approximation eliminates curvature terms, so the domain geometry is Cartesian rather than cylindrical. The excluded curvature terms have an explicit dependence on r, so they make the problem more challenging both analytically and numerically. In particular, in the wide-gap geometry (i.e. true Taylor Couette flow) the base angular velocity is a function of r, where in the thin-gap approximation the shear flow reduces to a linear profile.

We note several other important analytical studies of MRI saturation. Knobloch & Julien (2005) analyze the MRI in the strongly nonlinear regime, by following the already-developed MRI modes into asymptotic saturation. They find that this saturation proceeds via modification of the background shear. Knobloch & Julien consider a thin-gap regime as well, and so their theory

[1] Department of Astronomy, Columbia University, New York, NY
[2] Department of Astrophysics, American Museum of Natural History, New York, NY
[3] Department of Physics and Astronomy, Bates College

may be considered the strongly nonlinear analogue to the one developed here. Vasil 2015 examines the weakly nonlinear MRI in a thin-gap regime from a heuristic perspective, finding deep mathematical similarities between the MRI system and an elastodynamic instability. Several authors have investigated the behavior of the MRI when the boundary conditions are shear periodic, and so the MRI has no mechanism by which to modify the background shear flow profile. In this approximation linear MRI growth is dominated by channel modes, a type of MRI mode that, for periodic boundary conditions, are exact solutions of both the linear and nonlinear MRI equations (Goodman & Xu 1994). In this regime the MRI saturates via parasitic instabilities, which feed off and destroy the primary MRI modes. Analytical investigation of this case reveals that MRI saturation can be caused by parasitic Kelvin-Helmholtz and tearing mode instabilities, depending on parameter regime (Pessah 2010). The theory of MRI channel mode parasites is robust (see also Pessah & Goodman 2009, Latter et al. 2010, Rembiasz et al. 2016), but their importance may be overestimated by the local approximation Latter et al. 2015, and not germane to global analyses like the one presented here. Latter et al. 2015 gives a detailed analysis of the relation between local and global MRI modes.
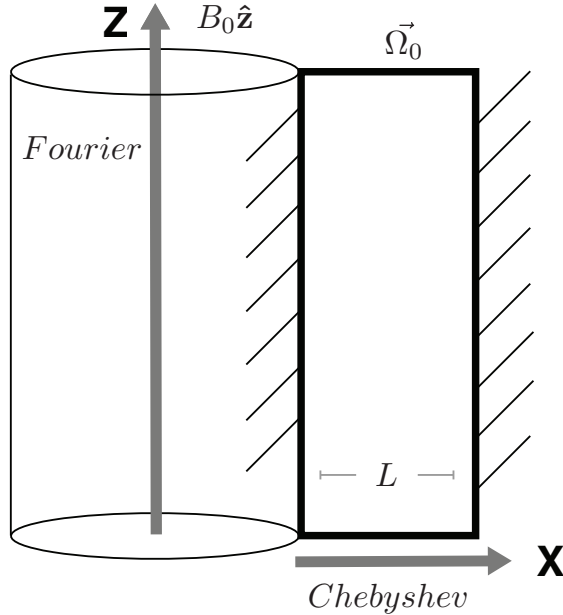
2. EQUATIONS

Fig. 1.— Schematic diagram of our set-up, an axisymmetric thin-gap Taylor Couette flow. We investigate a 2D slice of the X-Z (radial-vertical) plane. Our domain is represented by the bolded black box, of width L. The radial dimension is solved with a basis of Chebyshev polynomials, and the vertical dimension is solved on a Fourier basis.

The evolution of a conducting fluid is governed by the momentum and induction equations,

$$\partial_t \mathbf{u} + \mathbf{u} \cdot \nabla \mathbf{u} = -\frac{1}{\rho}\nabla P - \nabla \Phi + \frac{1}{\rho}\left(\mathbf{J} \times \mathbf{B}\right)$$
$$+ \nu \nabla^2 \mathbf{u} - 2\mathbf{\Omega} \times \mathbf{u} - \mathbf{\Omega} \times \left(\mathbf{\Omega} \times \mathbf{r}\right), \tag{1}$$

$$\partial_t \mathbf{B} = \nabla \times (\mathbf{u} \times \mathbf{B}) + \eta \nabla^2 \mathbf{B}, \tag{2}$$

where P is the gas pressure, ν is the kinematic viscosity, η is the microscopic diffusivity, $\nabla \Phi$ is the gravitational force per unit mass, and the current density is $\mathbf{J} = \nabla \times \mathbf{B}$. Equations 1 and 2 are subject to the magnetic solenoid and incompressibility constraints,

$$\nabla \cdot \mathbf{B} = 0 \tag{3}$$

$$\nabla \cdot \mathbf{u} = 0. \tag{4}$$

We axisymmetrically perturb all three vector components of each of the fluid quantities. We nondimensionalize the equations, with lengths nondimensionalized by L, velocities by $\Omega_0 L$, magnetic fields by B_0, and pressure by $\Omega_0^2 L^2 \rho_0$, where L is the channel width, Ω_0 is the rotation rate at the center of the channel, and ρ_0 is the constant pressure in the base state (see Figure 1). We define the Reynolds number, $\mathrm{Re} \equiv \Omega_0 L^2/\nu$, magnetic Reynolds number, $\mathrm{Rm} \equiv \Omega_0 L^2/\eta$, and a plasma beta parameter, $\beta \equiv \Omega_0^2 r_0^2/v_A^2$, where the Alfvén sped v_A is $v_A^2 = B_0^2/\rho_0$. The fluid symbols $\mathbf{u}$, $\mathbf{B}$, etc. will henceforth be used to refer to the nondimensional, perturbed quantities.

We define the flux function A and streamfunction Ψ, where A is the familiar two-dimensional vector potential. A and Ψ are scalar fields. The curl of A and the curl of Ψ are defined as the magnetic field and velocity, respectively, and so A and Ψ automatically satisfy our constraints (Equations 3 and 4).

A is thus related to the magnetic field as

$$\mathbf{B} = \begin{bmatrix} \partial_z A \\ B_y \\ -\partial_x A \end{bmatrix}, \tag{5}$$

and $\mathbf{\Psi}$ is defined analogously.

Our final equation set is

$$\partial_t \nabla^2 \Psi + J\left(\Psi, \nabla^2 \Psi\right) - 2\partial_z u_y =$$
$$\frac{2}{\beta}B_0 \partial_z \nabla^2 A + \frac{2}{\beta}J\left(A, \nabla^2 A\right) + \frac{1}{\mathrm{Re}}\nabla^4 \Psi \tag{6}$$

$$\partial_t u_{1y} + J\left(\Psi, u_y\right) + (2-q)\,\Omega_0 \partial_z \Psi =$$
$$\frac{2}{\beta}B_0 \partial_z B_y + \frac{2}{\beta}J\left(A, B_y\right) + \frac{1}{\mathrm{Re}}\nabla^2 u_y \tag{7}$$

$$\partial_t A = B_0 \partial_z \Psi + J\left(A, \Psi\right) + \frac{1}{\mathrm{Rm}}\nabla^2 A \tag{8}$$

$$\partial_t B_y \;=\; B_0 \partial_z u_y \;+\; J\left(A, u_y\right) \;-\; J\left(\Psi, B_y\right)$$
$$+ \; \frac{1}{\mathrm{Rm}}\nabla^2 B_y \;-\; q\Omega_0 \partial_z A, \quad (9)$$

where J is the Jacobian operator,

$$J\left(f, g\right) \equiv \partial_z f \partial_x g - \partial_x f \partial_z g, \qquad (10)$$

and $q = -d\ln\Omega/\ln R = 3/2$ is the dimensionless shear parameter such that the background velocity profile is $v_0 = q\Omega_0 x$.

Note that working in terms of the flux function raises the order of the first momentum equation.

The weakly nonlinear regime is where the MRI system is nonlinearly unstable to only the most unstable mode of the linear solution. We find the marginal state, where the most unstable linear MRI mode neither grows nor decays, for a given set of dimensionless parameters.

B_0 appears in Equations 6 - 9 because it is the nondimensionalized background field strength. Because we nondimensionalize B by the magnitude of the background field strength, $B_0 \equiv 1$. In order to study our system in the weakly nonlinear regime, we tune the background magnetic field down away from stability (recall that stronger vertical fields stabilize the MRI). We do so by substituting $B = B_0\left(1 - \epsilon^2\right)$. The degree of departure from the marginal state is measured by the small parameter ϵ. An $\mathcal{O}\left(\epsilon^2\right)$ weakening of the background magnetic field destabilizes a band of wave modes with width of $\mathcal{O}\left(\epsilon\right)$, which interact nonlinearly.

The destabilizing substitution is made, and Equations 6 - 9 are rewritten such that the fluid variables are contained in a state vector $\mathbf{V} = \left[\Psi, u_y, A, B_y\right]^{\mathrm{T}}$. This yields the system of equations

$$\mathcal{D}\partial_t \mathbf{V} + \mathcal{L}\mathbf{V} + \epsilon^2\widetilde{\mathcal{G}} = \mathbf{N}, \qquad (11)$$

where we leave the definition of the matrices $\mathcal{D}$, $\mathcal{L}$, and $\widetilde{\mathcal{G}}$ to Appendix B, and the detailed form of the nonlinear vector $\mathbf{N}$ to Appendix C. We solve this system subject to no-slip, perfectly conducting radial boundary conditions, defined as

$$\Psi = \partial_x\Psi = u_y = A = \partial_x B_y = 0. \qquad (12)$$

3. WEAKLY NONLINEAR ANALYSIS

We conduct a formal multiple scales analysis of this system. Our perturbations are characterized in terms of fast and slow-moving variables, in order to simultaneously track their evolution on two scales. The relative scalings of the fast and slow scales are determined as follows. When our four equations are linearized for axisymmetric perturbations of the form $e^{\sigma t + ik_x x + ik_z z}$, we can derive the linear dispersion relation, which is fourth order in σ (Appendix A). The fast and slow variables are then defined such that each of the temporal and spatial eigenvalues appear at the same lowest order in the linear dispersion relation. The scalings are

$$X \equiv \epsilon x, \; Y \equiv \epsilon y, \; Z \equiv \epsilon z, \; T \equiv \epsilon^2 t. \qquad (13)$$

Note that these are the same scalings as apply to Rayleigh-Bénard convection and hydrodynamic Taylor

Couette flow. Our x dimension, the direction of angular momentum transport, is analogous to the direction of temperature transport in the convection problem. In analogy to these problems, we posit slow variation in both Z and T. Each operator is expanded to reflect these scalings – for instance, ∂_z becomes $\partial_z + \epsilon\partial_Z$.

The multiple scale dependencies of our solution are encoded into an ansatz for the linear MRI solution at marginality,

$$\mathbf{V_1} = \alpha(T, Z)\mathbb{V}_{11}(x)e^{ik_c z} + c.c. + \beta(T, Z)\mathbb{U}_{11}(x) \quad (14)$$

where α is a slowly-varying amplitude equation and $c.c.$ denotes the complex conjugate. The x dependence is contained in $\mathbb{V}_{11} = (\Psi_{11}, u_{11}, A_{11}, B_{11})^{\mathbf{T}}$, and must be solved subject to the radial boundary conditions. The periodic vertical boundary conditions allow us to posit the z dependence, where k_c is the value of the vertical wavenumber at marginality. As noted by URM07, there exists a spatially constant neutral mode solution to the B_y equation, with $\mathbb{U}_{11} = (0, 0, 0, 1)^{\mathbf{T}}$. The amplitude $\beta(T, Z)$ encodes the slow evolution of this mode.

The state vector is expanded in a perturbation series in orders of ϵ,

$$\mathbf{V} = \epsilon\mathbf{V_1} + \epsilon^2\mathbf{V_2} + \epsilon^3\mathbf{V_3} + h.o.t. \qquad (15)$$

And our perturbed system is then expressed order by order as

$$\mathcal{O}(\epsilon) : \mathcal{L}\mathbf{V_1} + \mathcal{D}\partial_t\mathbf{V_1} = 0. \qquad (16)$$

$$\mathcal{O}(\epsilon^2) : \mathcal{L}\mathbf{V_2} + \widetilde{\mathcal{L}}_1\partial_Z\mathbf{V_1} = \mathbf{N_2} \qquad (17)$$

$$\mathcal{O}(\epsilon^3) : \mathcal{L}\mathbf{V_3} + \mathcal{D}\partial_T\mathbf{V_1} + \widetilde{\mathcal{L}}_1\partial_Z\mathbf{V_2} + \widetilde{\mathcal{L}}_2\partial_Z^2\mathbf{V_1} + \widetilde{\mathcal{G}}\mathbf{V_1} = \mathbf{N_3} \qquad (18)$$

The partial differential equations that comprise Equations 16 to 18 are solved in succession. The practical advantage of our ansatz construction (Equation 14) is clear: the separable x-dependence means that the radial boundary conditions are solved in only one dimension. Thus our analytical framework is able to side-step many of the resolution issues faced by multidimensional simulations. We are able to resolve even small-scale structure in the boundary layers of our domain, because we need only resolve it in one dimension. We solve the radial component of each equation using the open source pseudospectral code Dedalus. We compute the radial components on a grid of Chebyshev polynomials, as is appropriate for bounded one-dimensional domains (e.g. Boyd 2001). The nonuniform spacing of the Chebyshev grid allows us to resolve the boundary layers well on a 128-point grid.

To close the perturbation series we enforce a solvability criterion on Equation 18 (see Appendix B). This leads to an amplitude equation for $\alpha(T, Z)$ that governs the slow length- and timescale evolution of the system. This amplitude equation is

$$\partial_T\alpha = b\alpha + d\partial_Z^2\alpha - c\alpha\left|\alpha^2\right|, \qquad (19)$$
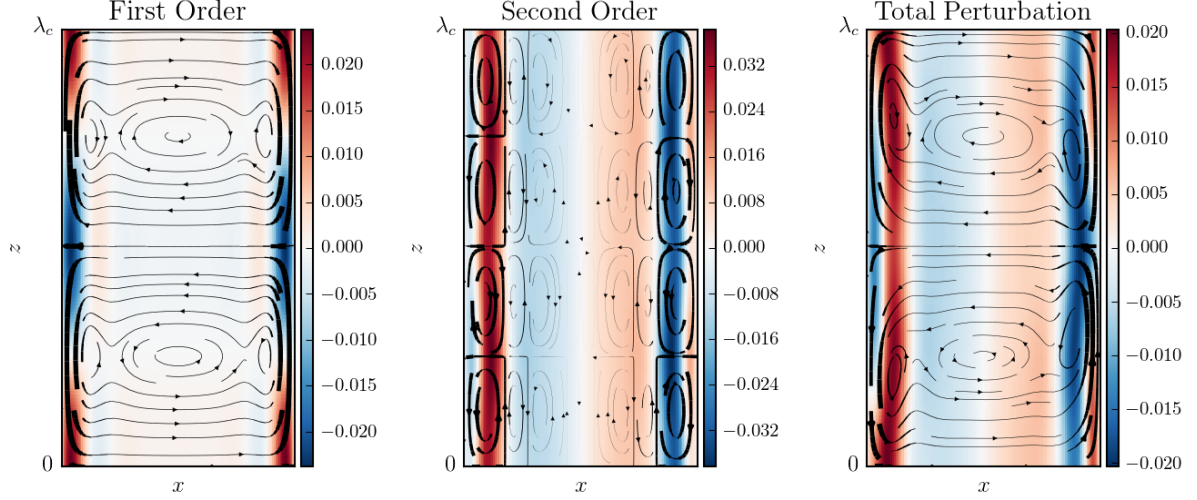
a real Ginzburg-Landau equation.

FIG. 2.— First order (left), second order (center), and total (right) velocity perturbations. Streamlines represent velocity in the vertical-radial plane, where thicker streamlines correspond to faster speeds. Colorbar represents azimuthal velocity.
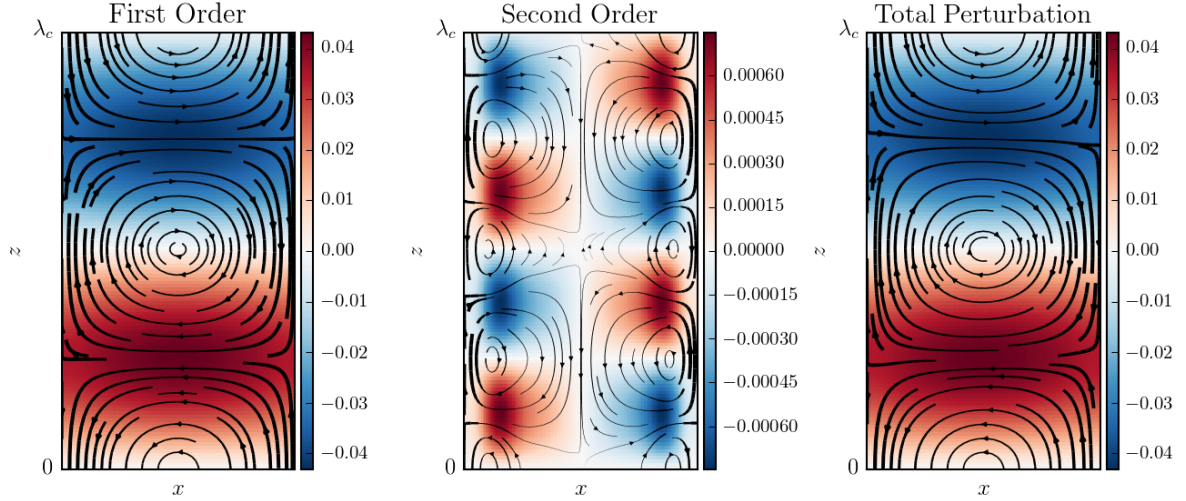

FIG. 3.— First order (left), second order (center), and total (right) magnetic field perturbations. Streamlines represent velocity in the vertical-radial plane, where thicker streamlines correspond to higher magnetic field strengths. Colorbar represents azimuthal magnetic field strength.

4. DISCUSSION

The fact that we find a Ginzburg-Landau equation for the amplitude is unsurprising: such an amplitude equation can be found in any system with Euclidean symmetry and a quadratic (or in our case quartic) maximum in growth rate with respect to k (Hoyle 2006). In this case, the Euclidean symmetry comes from axisymmetry in the x-z plane. In Paper II, we show that the same symmetry occurs in the axisymmetric global geometry as well. Figure ?? shows the saturated mean radial profiles of $u_0 - u_\phi = -q\Omega_0 x - u_\phi$ and each term in the steady state force balance (i.e. equation (7 with $\partial_t u_{1y} = 0$). In the bulk of the fluid away from the boundary layers, the saturated state shows reduced shear, with little diffusive contribution. However, the steep scaling of transport with Pm

Figure ?? shows B_z and the terms corresponding to steady state inductive balance (Equation 7 with $\partial_t B_y =$

0). Here, the instability acts to push magnetic field toward the boundaries in both the bulk and the boundary layers. Note also that the total magnetic energy in the B_z component is significantly larger than the initial condition. ? considered the saturation of a single, strongly super-critical MRI mode allowed to interact non-linearly only with itself and the mean. They considered two important cases, one in which the mean flow was forced to remain at its initial, quasi-Keplerian state for all time, and one in which the background flow was allowed to evolve. This is a crucial difference between the shearing box and our narrow-gap TC flow: perturbations in our simulation can adjust the background flow, whereas in a shearing box, the shear periodicity forbids perturbations from affecting the mean flow. In the case with a freely evolving background flow, Ebrahimi et al. (2009) found a saturated state quite similar to ours: field pushed to the boundaries, and a reduction in shear in the bulk of the

flow. Their flows have less pronounced boundary layers, likely because of their much larger $\mathrm{Pm} = 0.1 - 1$.

In the high Re and Rm limit, Vasil (2015) derives an amplitude equation considerably different than the one found here. By averaging in the z direction, he computes a mean-field equation with striking similarity to the buckling of an elastic beam under load. The most salient feature of his equation is its *non-local* character. Unlike the present work, which focuses on Keplerian rotation profiles with $q = 3/2$ with a critical B_0, Vasil (2015) focuses on a fixed B and a weakly destabilized shear profile. However, these differences are minor; the destabilizing parameter ϵ enters the analysis in the same quadratic proportion. Whether and how Vasil (2015)'s amplitude equation is equivalent to our own in the limit of dynamically important resistive and viscous effects is beyond the scope of this work.

The real Ginzburg-Landau equation describes the amplitude behavior of our system close to threshold. Although the form of the equation is generic, its coefficients depend on the specific physics of our system and govern its detailed evolution (see Appendix B). We simulate the evolution of the MRI amplitude equation by solving Equation 19 on a Fourier basis in Z using Dedalus. We initialize uniform random noise of amplitude -10^{-3} to $+10^{-3}$ in Z, and timestep the system using a four-stage, fourth-order Runge-Kutta integrator. We evolve the system for $100\Omega_0^{-1}$ in timesteps of $0.02\Omega_0^{-1}$. Results are shown in Figures 4 and 5. The system quickly organizes itself into rolls in Z bounded by the analytic saturation amplitude $\alpha_s = \sqrt{b/c}$. The specific geometry depends on the number of critical wavelengths $\lambda_{crit} = 2\pi/k_c$ that are initialized in Z. Figure 4 shows that a system with a height equal to two critical wavelengths will be modulated by simple rolls of sinusoidal amplitude. The saturation amplitude pattern becomes more complicated when more modes are allowed to interact. Figure 5 shows the evolution of a system of height $10\lambda_{crit}$. While still bounded by α_s, the saturation amplitude exhibits a nonlinear phase geometry due to the nonlinear interaction of modes in Z.

5. CONCLUSION

In this paper, we have constructed a weakly nonlinear analysis of the MRI using multiple-scales analysis. We find that the saturated state is a complex balance in which reduction of shear and amplification and redistribution of B_z combine to saturate the instability. We confirm the previous results of Umurhan et al. (2007b), including their $A^2 \propto \mathrm{Pm}^{4/3}$ scaling.

6. ACKNOWLEDGEMENTS

FIG. 4.— Evolution of the Ginzburg-Landau amplitude equation (Equation 19) on a Fourier Z domain of length $2\lambda_{crit}$, where $\lambda_{crit} = 2\pi/k_c$ is the critical wavelength of the system. Top left panel shows the evolution of the amplitude observable $\alpha\alpha^*$ on the full Z domain as a function of time T. Bottom left panel shows the amplitude $alpha$ at the final timestep shown, where the black line is the real part $\mathrm{Re}\{\alpha(t = t_{final})\}$ and the gray line is the imaginary part $\mathrm{Im}\{\alpha(t = t_{final})\}$. The final amplitude is bounded by the analytic saturation amplitude $\alpha_{saturation} = \pm\sqrt{b/c}$. Top right panel shows the evolution of the phase angle $\phi = \arctan(\mathrm{Im}(\alpha)/\mathrm{Re}(\alpha))$ on the same domain. Bottom panel shows the phase angle as a function of Z for the final timestep. Note that the phase angle is wrapped on a 2π domain, such that $\pi = -\pi$, as indicated by the circular colorbar.

FIG. 5.— Same as Figure 4 but for a Z domain of length $10\lambda_{crit}$.

APPENDIX

A. LINEAR DISPERSION RELATION

The linear dispersion relation, which determines the variable scalings in the multiple scales analysis. This relation is found by perturbing the linear system (Equation 16) with a small perturbation of the form $e^{\sigma t + i k_x x + i k_z z}$.

$$
\begin{aligned}
& \frac{B_0^4 k_x^2 k_z^4}{16\pi^2} + \frac{B_0^4 k_z^6}{16\pi^2} - \frac{B_0^2 \Omega_0 k_z^4 q}{2\pi} - 2\Omega_0 k_z^2 q\sigma^2 - \frac{4\sigma}{\mathrm{Rm}}\Omega_0 k_x^2 k_z^2 q - \frac{4\sigma}{\mathrm{Rm}}\Omega_0 k_z^4 q - \frac{2\Omega_0}{\mathrm{Rm}^2} k_x^4 k_z^2 q - \frac{4\Omega_0}{\mathrm{Rm}^2} k_x^2 k_z^4 q - \frac{2\Omega_0}{\mathrm{Rm}^2} k_z^6 q \\
& - k_x^2 \sigma^4 - k_z^2 \sigma^4 + 4k_z^2 \sigma^2 - \frac{2\sigma^3}{\mathrm{Rm}} k_x^4 - \frac{4\sigma^3}{\mathrm{Rm}} k_x^2 k_z^2 + \frac{8\sigma}{\mathrm{Rm}} k_x^2 k_z^2 - \frac{2\sigma^3}{\mathrm{Rm}} k_z^4 + \frac{8\sigma}{\mathrm{Rm}} k_z^4 - \frac{k_x^6 \sigma^2}{\mathrm{Rm}^2} - \frac{3\sigma^2}{\mathrm{Rm}^2} k_x^4 k_z^2 + \frac{4k_x^4}{\mathrm{Rm}^2} k_z^2 \\
& - \frac{3\sigma^2}{\mathrm{Rm}^2} k_x^2 k_z^4 + \frac{8k_x^2}{\mathrm{Rm}^2} k_z^4 - \frac{k_z^6 \sigma^2}{\mathrm{Rm}^2} + \frac{4k_z^6}{\mathrm{Rm}^2} - \frac{2\sigma^3}{\mathrm{Re}} k_x^4 - \frac{4\sigma^3}{\mathrm{Re}} k_x^2 k_z^2 - \frac{2\sigma^3}{\mathrm{Re}} k_z^4 - \frac{4k_x^6 \sigma^2}{\mathrm{ReRm}} - \frac{12 k_x^4 k_z^2 \sigma^2}{\mathrm{ReRm}} - \frac{12 k_x^2 k_z^4 \sigma^2}{\mathrm{ReRm}} \\
& - \frac{4k_z^6 \sigma^2}{\mathrm{ReRm}} - \frac{2k_x^8 \sigma}{\mathrm{ReRm}^2} - \frac{8k_x^6 k_z^2 \sigma}{\mathrm{ReRm}^2} - \frac{12 k_x^4 k_z^4 \sigma}{\mathrm{ReRm}^2} - \frac{8k_x^2 k_z^6 \sigma}{\mathrm{ReRm}^2} - \frac{2k_z^8 \sigma}{\mathrm{ReRm}^2} - \frac{k_x^6 \sigma^2}{\mathrm{Re}^2} - \frac{3\sigma^2}{\mathrm{Re}^2} k_x^4 k_z^2 - \frac{3\sigma^2}{\mathrm{Re}^2} k_x^2 k_z^4 - \frac{k_z^6 \sigma^2}{\mathrm{Re}^2} \\
& - \frac{2k_x^8 \sigma}{\mathrm{Re}^2 \mathrm{Rm}} - \frac{8k_x^6 k_z^2 \sigma}{\mathrm{Re}^2 \mathrm{Rm}} - \frac{12 k_x^4 k_z^4 \sigma}{\mathrm{Re}^2 \mathrm{Rm}} - \frac{8k_x^2 k_z^6 \sigma}{\mathrm{Re}^2 \mathrm{Rm}} - \frac{2k_z^8 \sigma}{\mathrm{Re}^2 \mathrm{Rm}} - \frac{k_x^{10}}{\mathrm{Re}^2 \mathrm{Rm}^2} - \frac{5k_x^8 k_z^2}{\mathrm{Re}^2 \mathrm{Rm}^2} - \frac{10 k_x^6 k_z^4}{\mathrm{Re}^2 \mathrm{Rm}^2} - \frac{10 k_x^4 k_z^6}{\mathrm{Re}^2 \mathrm{Rm}^2} \\
& - \frac{5k_x^2 k_z^8}{\mathrm{Re}^2 \mathrm{Rm}^2} - \frac{k_z^{10}}{\mathrm{Re}^2 \mathrm{Rm}^2} = 0
\end{aligned}
\tag{A1}
$$

B. DETAILED EQUATIONS

Here we detail the perturbation analysis described in Section 2. The linear system is described by Equation 11, where

$$
\mathcal{L} = \mathcal{L}_0 + \mathcal{L}_1 \partial_z + \mathcal{L}_2 \partial_z^2 + \mathcal{L}_3 \partial_z^3 + \mathcal{L}_4 \partial_z^4,
\tag{B1}
$$

$$
\widetilde{\mathcal{G}} = -\mathcal{G}\partial_z - \mathcal{L}_3 \partial_z^3,
\tag{B2}
$$

and the constituent matrices are defined as

$$
\mathcal{D} = \begin{bmatrix} \nabla^2 & 0 & 0 & 0 \\ 0 & 1 & 0 & 0 \\ 0 & 0 & 1 & 0 \\ 0 & 0 & 0 & 1 \end{bmatrix}
\tag{B3}
$$

$$
\mathcal{L}_0 = \begin{bmatrix} -\frac{1}{\mathrm{Re}}\partial_x^4 & 0 & 0 & 0 \\ 0 & -\frac{1}{\mathrm{Re}}\partial_x^2 & 0 & 0 \\ 0 & 0 & -\frac{1}{\mathrm{Rm}}\partial_x^2 & 0 \\ 0 & 0 & 0 & -\frac{1}{\mathrm{Rm}}\partial_x^2 \end{bmatrix}
\tag{B4}
$$

$$
\mathcal{L}_1 = \begin{bmatrix} 0 & -2 & -\frac{2}{\beta}\partial_x^2 & 0 \\ (2-q)\Omega_0 & 0 & 0 & -\frac{2}{\beta} \\ -1 & 0 & 0 & 0 \\ 0 & -1 & q\Omega_0 & 0 \end{bmatrix}
\tag{B5}
$$

$$
\mathcal{L}_2 = \begin{bmatrix} -2\frac{1}{\mathrm{Re}}\partial_x^2 & 0 & 0 & 0 \\ 0 & -\frac{1}{\mathrm{Re}} & 0 & 0 \\ 0 & 0 & -\frac{1}{\mathrm{Rm}} & 0 \\ 0 & 0 & 0 & -\frac{1}{\mathrm{Rm}} \end{bmatrix}
\tag{B6}
$$

$$
\mathcal{L}_3 = \begin{bmatrix} 0 & 0 & -\frac{2}{\beta} & 0 \\ 0 & 0 & 0 & 0 \\ 0 & 0 & 0 & 0 \\ 0 & 0 & 0 & 0 \end{bmatrix}
\tag{B7}
$$

$$
\mathcal{L}_4 = \begin{bmatrix} -\frac{1}{\mathrm{Re}} & 0 & 0 & 0 \\ 0 & 0 & 0 & 0 \\ 0 & 0 & 0 & 0 \\ 0 & 0 & 0 & 0 \end{bmatrix}
\tag{B8}
$$

$$\mathcal{G} = \begin{bmatrix} 0 & 0 & -\frac{2}{\beta}\partial_x^2 & 0 \\ 0 & 0 & 0 & -\frac{2}{\beta} \\ -1 & 0 & 0 & 0 \\ 0 & -1 & 0 & 0 \end{bmatrix} \tag{B9}$$

C. EXPANSION OF NONLINEAR TERMS

$$\mathbf{N} = \epsilon^2\mathbf{N_2} + \epsilon^3\mathbf{N_3} + \mathcal{O}(\epsilon^4) \tag{C1}$$

where

$$N_2^{(\Psi)} = J(\Psi_1, \nabla^2\Psi_1) - \frac{2}{\beta}J(A_1, \nabla^2 A_1) \tag{C2}$$

$$N_2^{(u)} = J(\Psi_1, u_1) - \frac{2}{\beta}J(A_1, B_1) \tag{C3}$$

$$N_2^{(A)} = -J(A_1, \Psi_1) \tag{C4}$$

$$N_2^{(B)} = J(\Psi_1, B_1) - J(A_1, u_1) \tag{C5}$$

and

$$N_3^{(\Psi)} = J(\Psi_1, \nabla^2\Psi_2) - \frac{2}{\beta}J(A_1, \nabla^2 A_2) + J(\Psi_2, \nabla^2\Psi_1) - \frac{2}{\beta}J(A_2, \nabla^2 A_1) + 2J(\Psi_1, \partial_z\partial_Z\Psi_1)$$
$$- 2\frac{2}{\beta}J(A_1, \partial_z\partial_Z A_1) + \widetilde{J}(\Psi_1, \nabla^2\Psi_1) - \frac{2}{\beta}\widetilde{J}(A_1, \nabla^2 A_1) \tag{C6}$$

$$N_3^{(u)} = J(\Psi_1, u_2) + J(\Psi_2, u_1) + \widetilde{J}(\Psi_1, u_1) - \frac{2}{\beta}J(A_1, B_2) - \frac{2}{\beta}J(A_2, B_1) - \frac{2}{\beta}\widetilde{J}(A_1, B_1) \tag{C7}$$

$$N_3^{(A)} = -J(A_1, \Psi_2) - J(A_2, \Psi_1) - \widetilde{J}(A_1, \Psi_1) \tag{C8}$$

$$N_3^{(B)} = J(\Psi_1, B_2) + J(\Psi_2, B_1) + \widetilde{J}(\Psi_1, B_1) - J(A_1, u_2) - J(A_2, u_1) - \widetilde{J}(A_1, u_1). \tag{C9}$$

$\mathbf{N_2}$ and $\mathbf{N_3}$ expand to become

$$\mathbf{N_2} = \alpha^2\mathbb{N}_{22}e^{i2k_cz} + |\alpha|^2\,\mathbb{N}_{20} + c.c. \tag{C10}$$

and

$$\mathbf{N_3} = \alpha^3\mathbb{N}_{33}e^{i3k_cz} + \alpha\partial_Z\alpha\mathbb{N}_{32}e^{i2k_cz} + \alpha\,|\alpha|^2\,\mathbb{N}_{31}e^{ik_cz} + \alpha\partial_Z\beta\widetilde{\mathbb{N}}_{31}e^{ik_cz} + \alpha^*\partial_Z\alpha\mathbb{N}_{30} + c.c. \tag{C11}$$

The second order nonlinear terms are

$$N_{22}^{(\Psi)} = ik_c\Psi_{11} \cdot \left(\partial_x^3\Psi_{11} - k_c^2\partial_x\Psi_{11}\right) - \partial_x\Psi_{11} \cdot \left(ik_c\partial_x^2\Psi_{11} - ik_c^3\Psi_{11}\right)$$
$$+ \frac{2}{\beta}\partial_x A_{11} \cdot \left(ik_c\partial_x^2 A_{11} - ik_c^3 A_{11}\right) - \frac{2}{\beta}ik_c A_{11} \cdot \left(\partial_x^3 A_{11} - k_c^2\partial_x A_{11}\right) \tag{C12}$$

$$N_{22}^{(u)} = ik_c\Psi_{11} \cdot \partial_x u_{11} - \partial_x\Psi_{11} \cdot ik_c u_{11} - \frac{2}{\beta}ik_c A_{11} \cdot \partial_x B_{11} + \frac{2}{\beta}\partial_x A_{11} \cdot ik_c B_{11} \tag{C13}$$

$$N_{22}^{(A)} = -ik_c A_{11} \cdot \partial_x\Psi_{11} + \partial_x A_{11} \cdot ik_c\Psi_{11} \tag{C14}$$

$$N_{22}^{(B)} = ik_c\Psi_{11} \cdot \partial_x B_{11} - \partial_x\Psi_{11} \cdot ik_c B_{11} - ik_c A_{11} \cdot \partial_x u_{11} + \partial_x A_{11} \cdot ik_c u_{11} \tag{C15}$$

$$N_{20}^{(\Psi)} = ik_c \Psi_{11} \cdot \left(\partial_x^3 \Psi_{11}^* - k_c^2 \partial_x \Psi_{11}^* \right) - \partial_x \Psi_{11} \cdot \left(ik_c^3 \Psi_{11}^* - ik_c \partial_x^2 \Psi_{11}^* \right)$$
$$+ \frac{2}{\beta} \partial_x A_{11} \cdot \left(ik_c^3 A_{11}^* - ik_c \partial_x^2 A_{11}^* \right) - \frac{2}{\beta} ik_c A_{11} \cdot \left(\partial_x^3 A_{11}^* - k_c^2 \partial_x A_{11}^* \right) \tag{C16}$$

$$N_{20}^{(u)} = ik_c \Psi_{11} \cdot \partial_x u_{11}^* + \partial_x \Psi_{11} \cdot ik_c u_{11}^* - \frac{2}{\beta} ik_c A_{11} \cdot \partial_x B_{11}^* - \frac{2}{\beta} \partial_x A_{11} \cdot ik_c B_{11}^* \tag{C17}$$

$$N_{20}^{(A)} = -ik_c A_{11} \cdot \partial_x \Psi_{11}^* - \partial_x A_{11} \cdot ik_c \Psi_{11}^* \tag{C18}$$

$$N_{20}^{(B)} = ik_c \Psi_{11} \cdot \partial_x B_{11}^* + \partial_x \Psi_{11} \cdot ik_c B_{11}^* - ik_c A_{11} \cdot \partial_x u_{11}^* - \partial_x A_{11} \cdot ik_c u_{11}^* \tag{C19}$$

and the third order nonlinear terms become

$$N_{31}^{(\Psi)} = ik_c \left(\Psi_{11} \cdot \partial_x^3 \Psi_{20} \right) + ik_c \left(\Psi_{11} \cdot \partial_x^3 \Psi_{20}^* \right) - ik_c \left(\Psi_{11}^* \cdot \partial_x^3 \Psi_{22} \right) - i2k_c \left(\partial_x \Psi_{11}^* \cdot \partial_x^2 \Psi_{22} \right)$$
$$+ i8k_c^3 \left(\partial_x \Psi_{11}^* \cdot \Psi_{22} \right) + i4k_c^3 \left(\Psi_{11}^* \cdot \partial_x \Psi_{22} \right) + \frac{2}{\beta} \left[-ik_c \left(A_{11} \cdot \partial^3 A_{20} \right) - ik_c \left(A_{11} \cdot \partial_x^3 A_{20}^* \right) \right]$$
$$+ \frac{2}{\beta} \left[ik_c \left(A_{11}^* \cdot \partial_x^3 A_{22} \right) + i2k_c \left(\partial_x A_{11}^* \cdot \partial_x^2 A_{22} \right) - i8k_c^3 \left(\partial_x A_{11}^* \cdot A_{22} \right) - i4k_c^3 \left(A_{11}^* \cdot \partial_x A_{22} \right) \right]$$
$$+ i2k_c \left(\Psi_{22} \cdot \partial_x^3 \Psi_{11}^* \right) - i2k_c^3 \left(\Psi_{22} \cdot \partial_x \Psi_{11}^* \right) - ik_c \left(\partial_x \Psi_{20} \cdot \partial_x^2 \Psi_{11} \right) + ik_c \left(\partial_x \Psi_{22} \cdot \partial_x^2 \Psi_{11}^* \right)$$
$$- ik_c \left(\partial_x \Psi_{20}^* \cdot \partial_x^2 \Psi_{11} \right) + ik_c^3 \left(\partial_x \Psi_{20} \cdot \Psi_{11} \right) + ik_c^3 \left(\partial_x \Psi_{20}^* \cdot \Psi_{11} \right) - ik_c^3 \left(\partial_x \Psi_{22} \cdot \Psi_{11}^* \right)$$
$$+ \frac{2}{\beta} \left[-i2k_c \left(A_{22} \cdot \partial_x^3 A_{11}^* \right) + i2k_c^3 \left(A_{22} \cdot \partial_x A_{11}^* \right) + ik_c \left(\partial_x A_{20} \cdot \partial_x^2 A_{11} \right) - ik_c \left(\partial_x A_{22} \cdot \partial_x^2 A_{11}^* \right) \right]$$
$$+ \frac{2}{\beta} \left[ik_c \left(\partial_x A_{20}^* \cdot \partial_x^2 A_{11} \right) - ik_c^3 \left(\partial_x A_{20} \cdot A_{11} \right) - ik_c^3 \left(\partial_x A_{20}^* \cdot A_{11} \right) + ik_c^3 \left(\partial_x A_{22} \cdot A_{11}^* \right) \right] \tag{C20}$$

$$N_{31}^{(u)} = ik_c \left(\Psi_{11} \cdot \partial_x u_{20} \right) + ik_c \left(\Psi_{11} \cdot \partial_x u_{20}^* \right) - ik_c \left(\Psi_{11}^* \cdot \partial_x u_{22} \right) - i2k_c \left(\partial_x \Psi_{11}^* \cdot u_{22} \right)$$
$$- ik_c \left(u_{11} \cdot \partial_x \Psi_{20} \right) - ik_c \left(u_{11} \cdot \partial_x \Psi_{20}^* \right) + ik_c \left(u_{11}^* \cdot \partial_x \Psi_{22} \right) + i2k_c \left(\partial_x u_{11}^* \cdot \Psi_{22} \right)$$
$$+ \frac{2}{\beta} \left[-ik_c \left(A_{11} \cdot \partial_x B_{20} \right) - ik_c \left(A_{11} \cdot \partial_x B_{20}^* \right) + ik_c \left(A_{11}^* \cdot \partial_x B_{22} \right) + i2k_c \left(\partial_x A_{11}^* \cdot B_{22} \right) \right]$$
$$+ \frac{2}{\beta} \left[ik_c \left(B_{11} \cdot \partial_x A_{20} \right) + ik_c \left(B_{11} \cdot \partial_x A_{20}^* \right) - ik_c \left(B_{11}^* \cdot \partial_x A_{20} \right) - i2k_c \left(\partial_x B_{11}^* \cdot A_{22} \right) \right] \tag{C21}$$

$$N_{31}^{(A)} = - ik_c \left(A_{11} \cdot \partial_x \Psi_{20} \right) - ik_c \left(A_{11} \cdot \partial_x \Psi_{20}^* \right) + ik_c \left(A_{11}^* \cdot \partial_x \Psi_{22} \right) + i2k_c \left(\partial_x A_{11}^* \cdot \Psi_{22} \right)$$
$$+ ik_c \left(\Psi_{11} \cdot \partial_x A_{20} \right) + ik_c \left(\Psi_{11} \cdot \partial_x A_{20}^* \right) - ik_c \left(\Psi_{11}^* \cdot \partial_x A_{22} \right) - i2k_c \left(\partial_x \Psi_{11}^* \cdot A_{22} \right) \tag{C22}$$

$$N_{31}^{(B)} = ik_c \left(\Psi_{11} \cdot \partial_x B_{20} \right) + ik_c \left(\Psi_{11} \cdot \partial_x B_{20}^* \right) - ik_c \left(\Psi_{11}^* \cdot \partial_x B_{22} \right) - i2k_c \left(\partial_x \Psi_{11}^* \cdot B_{22} \right)$$
$$- ik_c \left(B_{11} \cdot \partial_x \Psi_{20} \right) - ik_c \left(B_{11} \cdot \partial_x \Psi_{20}^* \right) + ik_c \left(B_{11}^* \cdot \partial_x \Psi_{22} \right) + i2k_c \left(\partial_x B_{11}^* \cdot \Psi_{22} \right)$$
$$- ik_c \left(A_{11} \cdot \partial_x u_{20} \right) - ik_c \left(A_{11} \cdot \partial_x u_{20}^* \right) + ik_c \left(A_{11}^* \cdot \partial_x u_{22} \right) + i2k_c \left(\partial_x A_{11}^* \cdot u_{22} \right)$$
$$ik_c \left(u_{11} \cdot \partial_x A_{20} \right) + ik_c \left(u_{11} \cdot \partial_x A_{20}^* \right) - ik_c \left(u_{11}^* \cdot \partial_x A_{22} \right) - i2k_c \left(\partial_x u_{11}^* \cdot A_{22} \right) \tag{C23}$$

REFERENCES

Balbus, S A and Hawley, J F, 1991, The Astrophysical Journal, 376, 214

Boyd, J P, 2001, Chebyshev and Fourier Spectral Methods, New York, Dover

Chandrasekhar, S. 1960, Proceedings of the National Academy of Sciences of the United States of America, 46, 253

Clark, S.E. and Oishi, J.S., 2016, in prep

Ebrahimi, F., Prager, S.C., Schnack, D.D, 2009, ApJ 698, 233

Goodman, J, Xu, G, 1994, ApJ, 432, 213

Hoyle, R. 2006, Pattern Formation, by Rebecca Hoyle, pp. 432. Cambridge University Press, March 2006. ISBN-10: 0521817501. ISBN-13: 9780521817509, 432

Knobloch, E, Julien K, 2005, Physics of Fluids, 17, 094106

Latter, H.N., Fromang, S., & Faure, J., 2015, MNRAS 453, 3257

Latter, H.N., Fromang, S., & Gressel, O., 2010, MNRAS 406, 848

Newell, A.C. & Whitehead, J.A. 1969, JFM 38, 279N

Pessah, M. E., 2010, ApJ, 716, 1012

Pessah, M. E., & Goodman, J., 2009, ApJ 698, L72

Rembiasz, T., Obergaulinger, M., Cerdá-Durán, P., Müller, E., & Aloy, M.A., 2016, MNRAS 456, 3782

Shakura, N I and Sunyaev, R A, Astronomy & Astrophysics, 1973, 24, 337

Umurhan, O M, Regev, O, Menou, K, 2007, Phys. Rev. Letters, 98, 034501

Umurhan, O M, Regev, O, Menou, K, 2007, Phys. Rev. E, 76, 036310

Vasil, G. M. 2015, RSPSA 471, 20140699